Journal of Power Sources 245 (2014) 362–370

Contents lists available at SciVerse ScienceDirect

Journal of Power Sources

journal homepage: www.elsevier.com/locate/jpowsour

High performance fluorine doped $(Sn,Ru)O_2$ oxygen evolution reaction electro-catalysts for proton exchange membrane based water electrolysis

Karan Kadakia [a], Moni Kanchan Datta [b,c], Oleg I. Velikokhatnyi [b,c], Prashanth Jampani [a], Sung Kyoo Park [b], Sung Jae Chung [d], Prashant N. Kumta [a,b,c,d,e,*]

[a] Department of Chemical and Petroleum Engineering, Swanson School of Engineering, University of Pittsburgh, PA 15261, USA
[b] Department of Bioengineering, Swanson School of Engineering, University of Pittsburgh, PA 15261, USA
[c] Center for Complex Engineered Multifunctional Materials, University of Pittsburgh, PA 15261, USA
[d] Department of Mechanical Engineering and Materials Science, Swanson School of Engineering, University of Pittsburgh, PA 15261, USA
[e] School of Dental Medicine, University of Pittsburgh, PA 15217, USA

HIGHLIGHTS

- Nano-structured $(Sn,Ru)O_2$:F thin films have been wet chemically synthesized.
- $(Sn_{0.80}Ru_{0.20})O_2$:10 wt% F films exhibit similar catalytic activity as RuO_2.
- $(Sn,Ru)O_2$:F thin films exhibit dura bility comparable to pure RuO_2.
- $(Sn,Ru)O_2$:F thin films are promising anode electro-catalysts for water electrolysis.

GRAPHICAL ABSTRACT

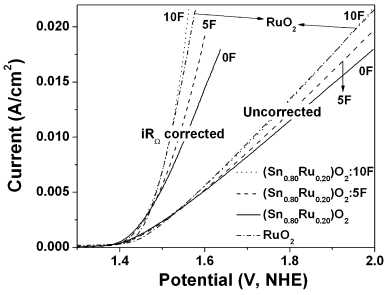

ARTICLE INFO

Article history:
Received 2 February 2013
Received in revised form
14 June 2013
Accepted 17 June 2013
Available online 27 June 2013

Keywords:
Oxygen evolution
Electrolysis
Electro-catalysts
Noble metal
Oxygen evolution reaction
Fuel cells

ABSTRACT

Identification of electro-catalysts containing non-noble metal or significantly reduced amounts of expensive noble metals (*e.g.* RuO_2) is highly desirable. Development of such a catalyst with comparable electrochemical performance to the standard noble metal oxide for proton exchange membrane (PEM) based water electrolysis would constitute a pioneering breakthrough in hydrogen generation by water electrolysis. In line with these goals, by exploiting a two-pronged theoretical first principles and experimental approach herein we demonstrate that a nano-structured solid solution of SnO_2:10 wt% F containing only 20 at.% RuO_2 [*e.g.* $(Sn_{0.80}Ru_{0.20})O_2$:10F] displays a remarkably similar electrochemical activity and moreover, comparable or even much improved electrochemical stability and durability compared to pure the noble metal counterpart, RuO_2. Density functional theory calculations have demonstrated direct dependence of the catalytic activity on the electronic structure peculiarities of the F-doped $(Ru,Sn)O_2$ which corresponds well with the experimental results.

1. Introduction

Hydrogen is considered as the ideal energy carrier and holds the potential to provide a clean, reliable, and affordable energy supply to meet the growing global demands of electric power and

* Corresponding author. Department of Chemical and Petroleum Engineering, Swanson School of Engineering, University of Pittsburgh, Pittsburgh, PA 15261, USA.
E-mail address: pkumta@pitt.edu (P.N. Kumta).

0378-7753/$ – see front matter © 2013 Elsevier B.V. All rights reserved.
http://dx.doi.org/10.1016/j.jpowsour.2013.06.099

transportation fuels [1–4]. Although a very attractive and lightweight fuel thus considered once to be the harbinger to the much touted hydrogen economy, a major limitation has been the identification and development of a viable and cost effective approach to hydrogen production. Splitting of water using electricity to produce hydrogen has always been considered a very promising way to produce hydrogen [1–6]. This involves however passage of an electric current through water causing its breakdown into hydrogen and oxygen popularly known as electrolysis. Electrolysis though less efficient than the direct chemical path however offers virtually no pollution or toxic byproducts if the electric current is generated using renewable energy (wind, solar, geothermal and hydropower) [1–9] making it a very attractive proposition. Progress in the production of hydrogen fuel by water electrolysis has however been hindered since the current electrolyzer technology costs are extremely prohibitive limiting the attainment of the targeted hydrogen production cost (<$3.00 gge^{-1} delivered) for distributed production systems. Currently established technologies for producing hydrogen require significant improvements in their technical and economic performance (efficiency and costs) if hydrogen is to be produced for energy use. Capital costs for current electrolyzer technologies are a major barrier to attaining the targeted hydrogen production costs.

High capital costs are incurred due to the use of expensive materials, relatively small systems, relatively low efficiencies, customized power electronics, and labor intensive fabrication [1–6]. PEM electrolyzers have more advantages as compared to alkaline water electrolyzers viz. safety, reliability, hydrogen purity, less energy consumption and better efficiency. Thus fabrication of proton exchange membrane (PEM) electrolysis cells utilizing non-precious metal catalysts for electrodes with high activity and durability would significantly decrease the overall capital costs. However, it is unlikely that a non-noble metal based catalyst will be identified for PEM systems, nevertheless approaches to decrease noble metal loading are highly desirable and need to be identified. Decreasing the noble metal loading as well as improving the catalytic activity and durability could be achieved using novel synthesis techniques to generate high specific surface area (HSA) nanostructured electro-catalyst, or improved low cost support structure (diluents) for electro-catalyst [10–15]. Identification and utilization of less expensive, more durable materials as supports or diluents for expensive electro-catalyst that are simpler and easier to manufacture would certainly help reduce the overall capital costs.

In PEM based water electrolysis, rutile-type noble metal oxides, IrO_2 and RuO_2, have been identified as a promising oxygen electrode anode catalyst [10–29]. Although RuO_2 is not as durable as IrO_2 during PEM electrolysis operation conditions, it has been found to exhibit better catalytic activity than IrO_2 [25,30]. It has also been reported [17,25,31–36] that the stability of RuO_2 as an electrocatalyst can be significantly improved by doping with other oxides such as SnO_2, Co_3O_4, MnO_2, Ta_2O_5 etc. However, such mixed oxides result in a decrease in active surface area and electrical conductivity with increase in the amount of the less economical and also non-conductive metal oxide. Hence no beneficial effect on the electrochemical performance of the catalyst is achieved with the addition of less expensive oxides beyond a percolation threshold limit (*e.g.* above 50 at.%). For example, it has been reported previously [33,36–39] and identified by the present authors that the electrochemical activity of a solid solution of RuO_2 and SnO_2 [(Sn,Ru)O_2], tested at 40 °C in 1 N H_2SO_4 solution, shows a drastic degradation of the electrochemical activity above 50 at.% SnO_2 thus requiring larger noble metal oxide contents to achieve the desired catalytic activity and stability. Accordingly, the polarization curve of (Sn,Ru)O_2 without ohmic loss correction, shown in Fig. 1, shows the current density of ($Sn_{0.8}Ru_{0.2}$)O_2 at 1.75 V (~0.0098 A cm^{-2} at 1.75 V) to be

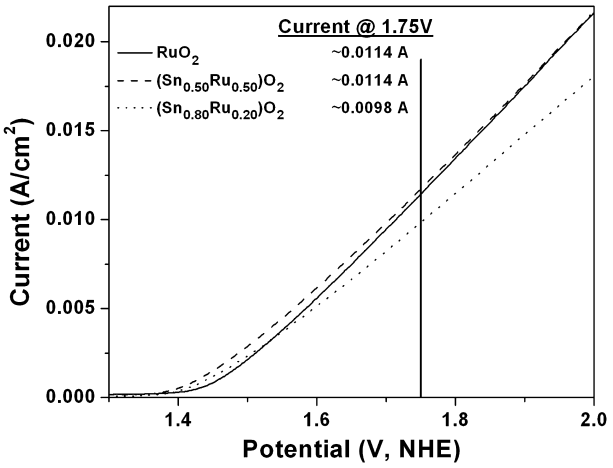

Fig. 1. The polarization curve of (Sn,Ru)O_2 of different compositions along with pure RuO_2 conducted in the presence of 1 N H_2SO_4 solution at 40 °C with a scan rate of 1 mV s^{-1}.

~15% lower than that of pure RuO_2 (~0.0114 A cm^{-2} at 1.75 V) obtained by a reduction of noble metal oxide loading by 80 at.%.

Recently, we have reported [40] that F doping to the solid solution of IrO_2 and corrosion resistant oxide such as SnO_2, Nb_2O_5 and Ta_2O_5 shows a drastic improvement in electrochemical activity and durability with significant reduction in IrO_2 content. The studies show that this may be due to increase in the electrical conductivity and shifting of the d-band center toward pure IrO_2. Exploiting a similar concept, we have studied F-doped ($Sn_{0.80}Ru_{0.20}$)O_2 for the first time to explore improvement in the electrochemical activity and demonstrate performance similarity to pure RuO_2 when the precious metal loading is reduced by almost 80%. In order to demonstrate this remarkable result, a homogeneous solid solution of SnO_2:F and RuO_2 [(Sn,Ru)O_2:F] of nominal compositions ($Sn_{0.8}Ru_{0.2}$):*x* wt% F with $x = 0$, 5, 10 and 15, has been synthesized by thermal decomposition of a mixture of metal salt precursors on Ti foil as a thin film anode electro-catalyst for PEM based electrolysis. In addition, to obtain a better understanding of the fundamental electrochemical activity and long term stability of the (Sn,Ru)O_2:F electro-catalyst, first-principles calculations of the total energies and electronic structures of the model systems with chemical compositions similar to those of the above mentioned experimentally synthesized materials have been carried out to complement the present experimental study.

2. Experimental and computational details

2.1. Preparation of the electrodes

Ruthenium trichloride [$RuCl_3$, 99.9%, Alfa Aesar], tin (II) chloride dihydrate [$SnCl_2 \cdot 2H_2O$, 98%, Alfa Aesar] and ammonium fluoride [NH_4F, 98%, Alfa Aesar] were used as the sources for Ru, Sn and F, respectively. Stock solution corresponding to $RuCl_3$ and $SnCl_2 \cdot 2H_2O$ of the desired compositions were dissolved in absolute ethanol (200 proof, Fisher Scientific) inside an atmosphere controlled glove box (MBraun Unilab Workstation (1200/780)) to prevent any undesired side reaction. Concurrently, NH_4F was dissolved in ethanol-DI water mixture (5:1 volume ratio). The stock solutions $RuCl_3$, $SnCl_2 \cdot 2H_2O$ and NH_4F of desired compositions are then mixed together to synthesize the various (Sn,Ru)O_2:F electro-catalyst. Following this the resulting solution was then spin coated on pre-treated titanium substrates (99.99%, 0.005 in thick, Alfa Aesar) of ~1 cm^2 areas (Speciality coating Systems Inc, Model P6712) with

rotating speed of 500 rpm for 10 s. Prior to coating, the Ti substrate was sand blasted and then etched in boiling HCl (30%) for 30 min in order to ensure maximum adhesion of the coating. The HCl treated Ti foil was washed with purified water generated by the Milli-Q system (18 MΩ cm deionized water, Milli-Q Academic, Millipore) and dried at 130 °C before coating. The thin film precursors deposited on the pretreated titanium substrate were dried at 60 °C for 2 h. Following this treatment, they were thermally treated at 723 K for 4 h in air to decompose the precursors and consequently generate (Sn,Ru)O_2:F film of different compositions on the Ti foils. The loading of the active (Sn,Ru)O_2:F deposited on the Ti foil is ~0.3 mg cm^{-2} irrespective of the different compositions. The loading has been determined by measuring the difference in weight between the coated and the uncoated Ti foils using a 6 digit high precision micro balance. The coating and drying step has been performed until the exact amount is coated to correspond to the desired active catalyst loading of ~0.3 mg cm^{-2}.

2.2. Materials characterization

In order to perform qualitative phase analysis, the (Sn,Ru)O_2:F thin film electrode of different compositions coated on Ti foil were characterized by X-ray diffraction (XRD) using Philips XPERT PRO system employing CuK_α ($\lambda = 0.15406$ nm) radiation at an operating voltage and current of 45 kV and 40 mA, respectively. The XRD peak profile of (Sn,Ru)O_2:F film was analyzed using the Pseudo-Voigt function to determine the Lorentzian and Gaussian contribution of the peak [41,42]. The integral breadth of the Lorentzian contribution, determined from peak profile analysis using the single line approximation method after eliminating the instrumental broadening and lattice strain contribution, is used in the Scherrer formula to calculate the effective crystallite size of the (Sn,Ru)O_2:F electrode of different compositions [41,42]. To investigate the microstructure of the thin film electrodes, scanning electron microscopy (SEM) was conducted. Quantitative elemental analysis and distribution of elements (by X-ray mapping) was obtained by using the energy dispersive X-ray spectroscopy (EDX) analyzer attached with the SEM machine. Philips XL-30FEG equipped with an EDX detector system comprised of an ultrathin beryllium window and Si(Li) detector operating at 20 kV was employed for the secondary electron (SE) image, elemental and X-ray mapping analyses. In order to evaluate the particle size and the structure of the thin film particles, TEM analysis has been conducted using JEOL 4000EX operating at 400 kV. The particles for the TEM analysis are obtained by mechanically abrading the powders from top of the thin films synthesized by spin coating techniques.

The electrochemical activity of RuO_2 and (Sn,Ru)O_2:F of different compositions, used as the catalyst in the oxygen evolution anode for PEM based water electrolysis, was conducted in an electrochemical workstation (VersaSTAT 3, Princeton Applied Research) using a three electrode cell configuration. The electrochemical reactivity and electrochemical kinetics of the electro-catalyst has been determined by conducting a combination of cyclic voltammetry, linear polarization and electrochemical impedance spectroscopy (EIS) analyses. A solution containing 1 N sulfuric acid (H_2SO_4) was used as the electrolyte while also serving as the source of the fuel. The H_2SO_4 sulfuric acid solution is kept at a constant temperature of 40 °C using a Fisher Scientific 910 Isotemp refrigerator circulator.

Thin films of RuO_2 and (Sn,Ru)O_2:F of different F compositions coated on Ti foil were used as the working electrode with an exposed surface area ~1 cm^2 comprised of a total loading of ~0.3 mg cm^{-2} for each system. The polarization curve was recorded employing a scanning rate of ~1 mV s^{-1} using platinum as the counter electrode and Hg/Hg_2SO_4 as the reference electrode that has a potential of +0.65 V with respect to the Normal hydrogen electrode (NHE). EIS has been used to determine the solution resistance, electrode resistance and the polarization resistance of the electro-catalyst using a suitable circuit model such as $R_s(R_eQ_1)(R_{ct}Q_{dl})$, where R_s is the solution resistance, R_e is the electrode resistance, R_{ct} is the charge transfer resistance, Q_1 is the constant phase element (CPE) and Q_{dl} includes both the double layer capacitance (C_{DL}) and pseudocapacitance (C_{PC}) [18,43]. The ohmic resistance (R_Ω) has been be used to perform the ohmic loss (iR_Ω) correction, whereas the polarization resistance has been used to understand the electrochemical activity of the electro-catalyst. The Tafel plot after iR_Ω correction given by the following equation $\eta = b \log i + a$ (plot of overpotential, η, vs. log current, log i) and the corresponding Tafel slope (b), determined from the corresponding polarization curve, has been used to determine the reaction kinetics [44,45]. Electrochemical impedance spectroscopy has been carried out in the frequency range of 100 mHz–100 kHz using the electrochemical work station (VersaSTAT 3, Princeton Applied Research). Impedance data has been modeled by using ZView software from Scribner Associates. In order to study the accelerated life test (durability) of the (Sn,Ru)O_2:F electrode as an anode for PEM based water electrolysis, chronoamperometry (CA) (current vs. time) of selected samples has been performed for 12 h using 1 N H_2SO_4 as the electrolyte utilizing the same three electrode cell configuration at a temperature of 40 °C. Elemental analysis of the electrolyte (H_2SO_4), collected after 12 h of CA testing, was performed by inductively coupled plasma optical emission spectroscopy (ICP-OES, iCAP 6500 duo Thermo Fisher) in order to determine the amount of ruthenium leached out in the solution from the electrode thus providing a measure of the electrochemical stability of the electro-catalyst.

2.3. Computational methodology and details

To obtain deeper insight into the intrinsic properties of the RuO_2–SnO_2 pure and F-doped solid solutions a continuous string of first-principles studies have been conducted using Density Functional Theory methodology implemented in the Vienna Ab-initio Simulation Package (VASP) [46–48]. The projector augmented-wave (PAW) method with the generalized gradient approximation (GGA) [49] for conducting the exchange-correlation corrections has been used for calculation of the total energies, electronic structures and optimized lattice parameters of the different model materials with chemical compositions similar to those compounds studied experimentally and described above in the present work. All the atoms were allowed to relax with the residual force components on each atom to be lower than ~0.01 eV $Å^{-1}$ $atom^{-1}$, thus resulting in the accurate determination of the atomic positions and hence, the total energy of the whole system. The Monkhorst–Pack scheme was used to sample the Brillouin Zone (BZ) and generate the k-point grid for the solids and the different isolated atoms used in the present study. A choice of the appropriate number of k-points in the irreducible part of the BZ was based on convergence of the total energy to be 0.1 meV $atom^{-1}$. Standard PAW potentials were employed for the elemental constituents of all pure and doped compounds in the study.

As a model system a 12-atom supercell containing two rutile-type unit cells has been constructed to represent the following compositions of the materials considered: RuO_2; $Sn_{0.25}Ru_{0.75}O_2$; $Sn_{0.5}Ru_{0.5}O_2$; $Sn_{0.75}Ru_{0.25}O_2$; $Sn_{0.75}Ru_{0.25}O_{1.5}F_{0.5}$; and $Sn_{0.75}Ru_{0.25}O_{1.0}F_{1.0}$. The last two compositions correspond to 6.4 and 12.7 wt% of F respectively. It should also be noted that for Sn–Ru–O–F compositions, the corresponding atomic distributions are ambiguous and can be represented by different spatial configurations. To eliminate this uncertainty several atomic configurations for each

given composition have been constructed and only those configurations corresponding to minimal total energies have been selected for further electronic structure analysis of these specific compositions of the binary oxides.

3. Results and discussion

Fig. 2(a) shows the XRD patterns of thin films of RuO_2 and SnO_2 synthesized by thermal decomposition of $RuCl_3$ and $SnCl_2 \cdot 2H_2O$ ethanol solution, respectively, coated on Ti foil following heat treatment at 723 K for 4 h. The XRD patterns of the RuO_2 and SnO_2 thin film show tetragonal structure as expected. The XRD patterns of $(Sn_{0.8}Ru_{0.2})O_2$:F with different F compositions (0, 5, 10, 15 wt%), shown in Fig. 2(b) and indicated by filled black circles, also show the peaks corresponding to tetragonal structure which suggest the formation of complete solid solution without any undesirable phase separation (*e.g.* $SnO_2 + RuO_2$). Formation of metastable solid solution between RuO_2 and SnO_2 as well as in the other oxide systems such as RuO_2, SbO_2, and SnO_2 has been reported by other researchers [10,32,33]. However, it should be noted that (Sn,Ru)O_2:15 wt% F shows an extra peak for SnO_2 which indicates that excess F substitution leads to phase separation. The calculated effective crystallite size for all of the (Sn,Ru)O_2:F films is in the range of ~5–10 nm which is comparable with (Sn,Ru)O_2 suggesting that F^- doping has no significant effect on the refinement of crystallite size of (Sn,Ru)O_2. The presence of elemental Sn, Ru and O in the (Sn,Ru)O_2:F film of different compositions has been confirmed using energy dispersive X-ray spectroscopy (EDX) configured to the SEM, although as expected, the presence of F could not be detected. The SEM image along with elemental X-ray mapping (Fig. 3(a)) and EDX analysis (Fig. 3(b)) for a representative (Sn,Ru)O_2:F film containing 10 wt% F indicates the presence of the characteristic "mud crack" morphology of the (Sn,Ru)O_2:F film coated on Ti foil (Fig. 3(a)), and also validates the presence of Sn, Ru and O (Fig. 3(a)) which are homogeneously distributed within the (Sn,Ru)O_2:F particles (see the elemental dot maps in Fig. 3(a)) without being segregated on any specific site or on any particular region of the particle. Quantitative analysis of the elemental composition of the representative (Sn,Ru)O_2:10F films obtained by EDX (Fig. 3(b)), shows that the measured elemental composition of Sn and Ru which is 77.4 at.% and 22.6 at.% respectively are expectedly close to the nominal composition. Elemental composition of the other electro-catalysts was also measured by EDX and was found to be similar to the nominal composition. The bright field TEM image of (Sn,Ru)O_2:F particles, shown in Fig. 3(c), collected from the (Sn,Ru)O_2:10 wt% F film confirms nanostructured fine particles of ~10–15 nm corresponding to the (Sn,Ru)O_2:F solid solution.

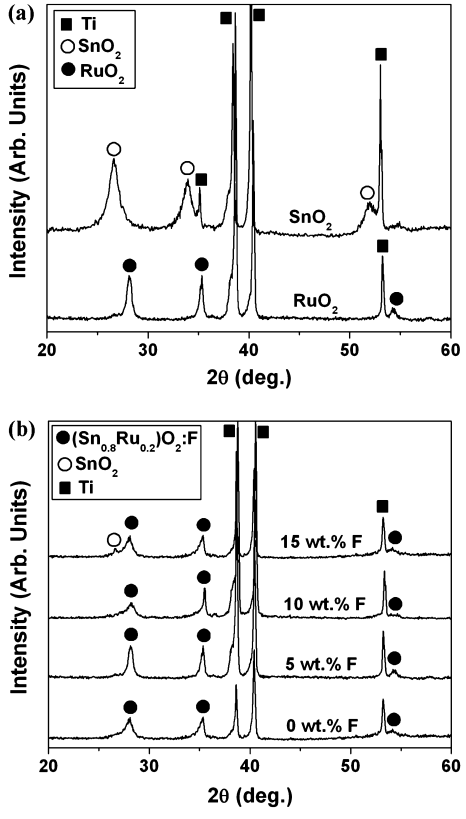

Fig. 2. XRD patterns of thin film RuO_2 and SnO_2 (a), and $(Sn_{0.8}Ru_{0.2})O_2$:F for different F compositions (b) coated on Ti foil.

The electrochemical activity of RuO_2 and (Sn,Ru)O_2:F thin films of different composition has been studied as an OER anode electrocatalyst for PEM based water electrolysis. It should be noted that the linear polarization curve and non-linear Tafel plots are typically most often encountered due to a large contribution of ohmic resistance (R_Ω) which mainly arises due to the solution resistance of the electrolyte (solution resistance, R_s), the oxide film electrode resistance (R_e) and the accumulation of oxygen gas bubble covering the electrode surface during water electrolysis occurring at higher current densities (bubble resistance, R_{bub}) [30,31]. These contributions were also observed in the present study. In order to evaluate the inherent electrochemical property/electrode kinetics of the electro-catalyst studied herein, the polarization curve of different samples, conducted in the presence of 1 N H_2SO_4 solution at 40 °C with a scan rate of 1 mV s^{-1}, is plotted after appropriately correcting for the total ohmic loss (iR_Ω). The total ohmic loss (iR_Ω) is the sum value of the solution resistance (R_s) and the electrode resistance (R_e). The value of R_s and R_e, respectively of the different samples, tabulated in Table 1, is obtained from electrochemical impedance spectroscopy (EIS) measurements conducted at different potentials with respect to NHE at 40 °C.

Fig. 4 shows the electrochemical impedance plot of RuO_2 and (Sn,Ru)O_2:F obtained at 1.6 V, the typical voltage selected for evaluating the optimal performance of the catalyst at 40 °C in the presence of 1 N H_2SO_4 solution in the frequency range of 100 mHz–100 kHz. The impedance parameters (Table 1) are obtained by fitting the experimental data (Fig. 4) using the ZView software from Scribner Associates with a circuit model $R_s(R_eQ_1)(R_{ct}Q_{dl})$, where R_s is the solution resistance, R_e is the electrode resistance, R_{ct} is the charge transfer resistance, Q_1 is the constant phase element (CPE) and Q_{dl} includes contributions from both the double layer capacitance and pseudocapacitance, respectively [28,29]. R_s is the resistance encountered at high frequencies due to charge transfer in the solution. R_e is the resistance faced in the circuit due to electron transfer from the electrode to the current collector (*i.e.* our coated Ti foil substrate). It has been observed that the solution resistance (R_s) and the electrode resistance (R_e) of RuO_2 and (Sn,Ru)O_2:F for the different F containing compositions is unchanged with change in potential. As shown in Table 1, the value of the electrode resistance (R_e) of (Sn,Ru)O_2:F decreases with increase in F content in the parent (Sn,Ru)O_2 lattice which may arise due to the improved electronic conductivity of (Sn,Ru)O_2:F with increase in F. Consequently, (Sn,Ru)O_2:F with 10 wt% F exhibits almost identical electrode resistance ($R_e \sim 1.5\ \Omega\ cm^{-2}$) as pure RuO_2 ($R_e \sim 1.1\ \Omega\ cm^{-2}$) suggesting the identical electronic conductivity of both systems. The low frequency EIS plot of pure RuO_2 and (Sn,Ru)O_2:F, shown in Fig. 4, shows a well formed semicircle related to OER and also indicates that the diameter of the low frequency semicircle typically a measure of the polarization resistance (R_{ct}) decreases (Table 1) with

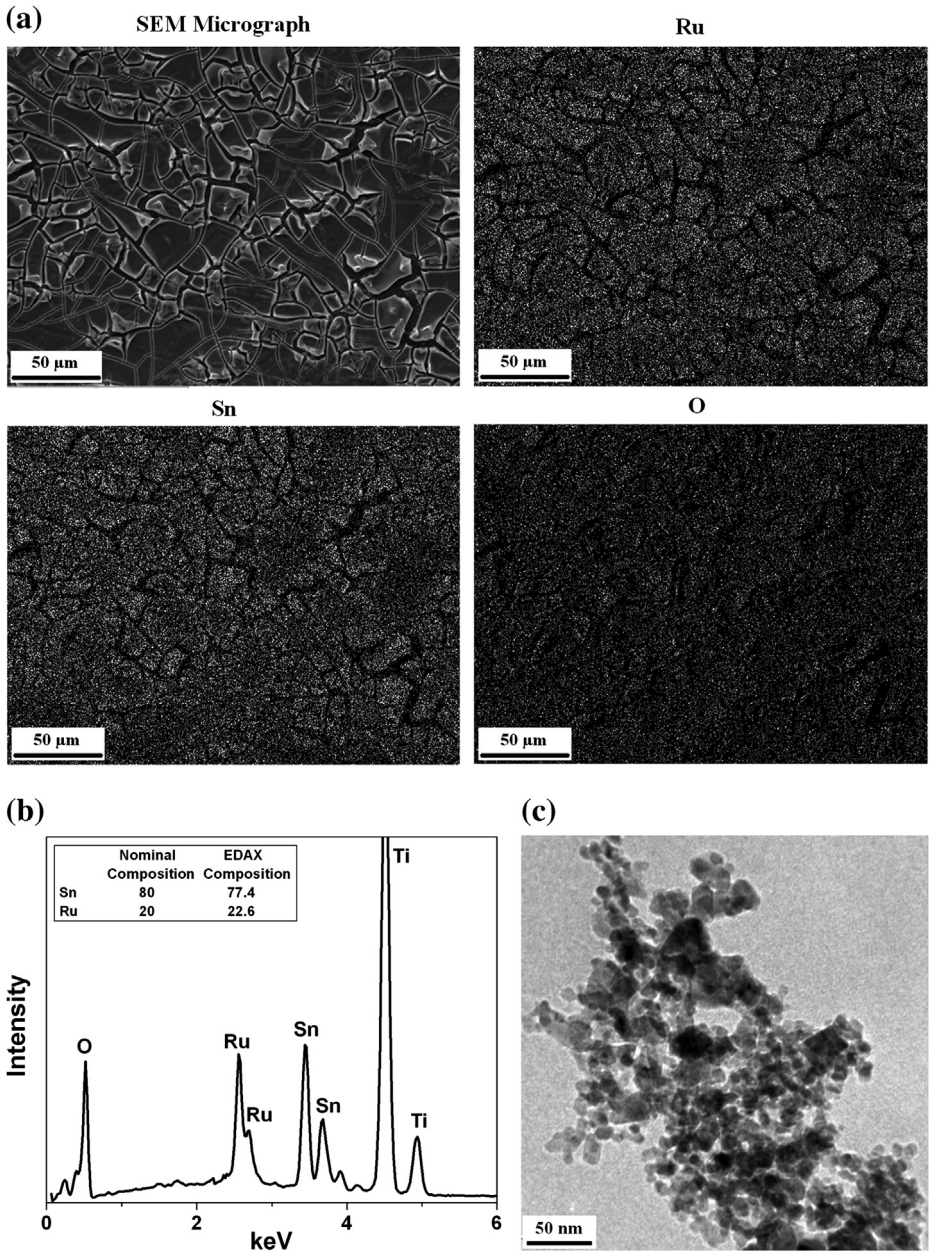

Fig. 3. The SEM micrograph along with X-ray mapping of Ru, Sn and O (a), and EDAX (b) of $(Sn_{0.8}Ru_{0.2})O_2$:10F film. (c) The TEM bright field image of $(Sn_{0.8}Ru_{0.2})O_2$:10F film showing the presence of fine nanoparticles.

increase in F. The above results therefore clearly suggests that the electrochemical activity of $(Sn_{0.8}Ru_{0.2})O_2$:F increases with increase in F and moreover, the polarization resistance (R_{ct}) value of $(Sn_{0.8}Ru_{0.2})O_2$:10F is similar (~4.2 Ω) to that of pure RuO_2 (~3.1 Ω) which further indicates that both systems will likely exhibit almost equivalent electrocatalytic activity as detailed below.

Table 1
Impedance parameters and Tafel slope of RuO_2 and $(Sn,Ru)O_2$:F obtained fitting the experimental EIS data to the equivalent circuit $R_s(R_eC_1)(R_{ct}Q_{ct})$ and Tafel plot, respectively.

Composition	R_s (Ω)	R_e (Ω)	R_{ct} (Ω)	Tafel slope (b)
RuO_2	13.5	1.1	3.10	77
$(Sn_{0.8}Ru_{0.2})O_2$	12.3	3.2	4.96	76
$(Sn_{0.8}Ru_{0.2})O_2$:5F	10.6	2.0	4.65	67
$(Sn_{0.8}Ru_{0.2})O_2$:10F	12.3	1.5	4.17	65

The polarization curve of pure SnO_2:F and RuO_2 film, before and after ohmic resistance correction ($iR_\Omega = iR_s + iR_e$) without considering the bubble resistance, conducted in the presence of 1 N H_2SO_4 solution at 40 °C with a scan rate of 1 mV s^{-1}, is shown in Fig. 5. The polarization curve of SnO_2:F in Fig. 5 as expected shows no catalytic activity at all for water electrolysis. On the other hand, nanocrystalline, undoped and pure RuO_2 clearly indicates the occurrence of the water splitting (oxygen evolution reaction) reaction at a potential of ~1.43 V vs. NHE. The current density at ~1.55 V (vs. NHE), the typical voltage selected to evaluate the electrochemical activity for water electrolysis obtained from iR_Ω corrected plot is ~0.0176 ± 0.001 A cm^{-2} at 40 °C with a total loading ~0.3 mg cm^{-2} of RuO_2. The polarization curve for the various $(Sn,Ru)O_2$:F film compositions containing different amounts of F before and after iR_Ω correction, plotted in Fig. 6 also shows that water splitting (oxygen evolution reaction) occurs at the potential

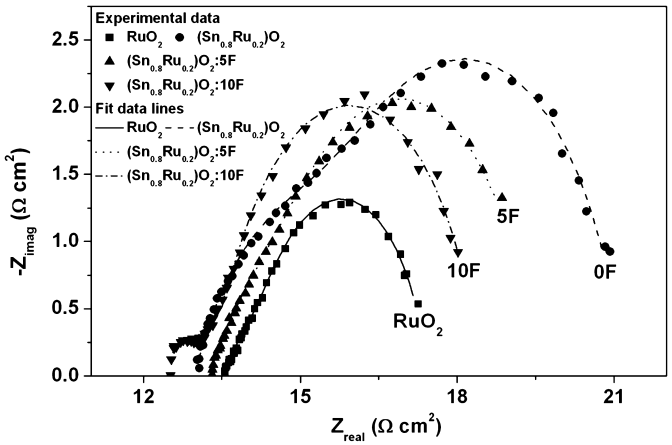

Fig. 4. The electrochemical impedance plot of (Sn,Ru)O_2:F and RuO_2 obtained at 1.6 V at 40 °C in the presence of 1 N H_2SO_4 solution in the frequency range of 100 mHz–100 kHz.

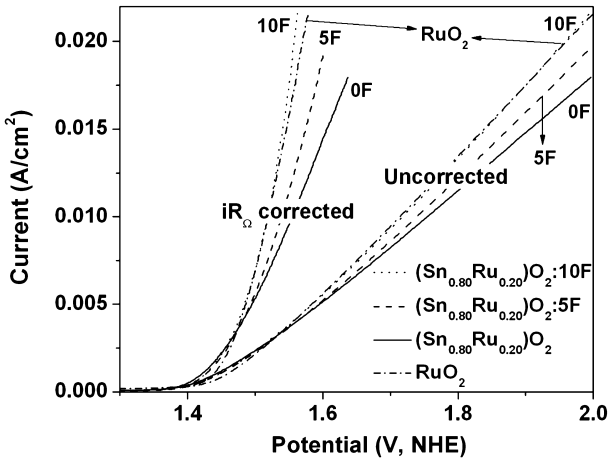

Fig. 6. The polarization curve of pure $(Sn_{0.8}Ru_{0.2})O_2$:F film of different F compositions conducted in the presence of 1 N H_2SO_4 solution at 40 °C with a scan rate of 1 mV s^{-1} before and after iR_Ω correction.

of ~1.4 V (vs. NHE) irrespective of the composition which is identical to that of pure RuO_2. Furthermore, the current density at ~1.55 V (vs. NHE) obtained from iR_Ω corrected plot for undoped (Sn,Ru)O_2 solid solution (0% F) with an identical total loading of ~0.3 mg cm^{-2} is ~0.009 ± 0.0001 A cm^{-2} at 40 °C which is almost 50% of that of pure RuO_2. However, as shown in Fig. 6, the current density of (Sn,Ru)O_2:F increases with increase in F content. In fact, for (Sn,Ru)O_2:F containing 10 wt% F the current density at ~1.55 V (vs. NHE) is ~0.0175 ± 0.001 A cm^{-2} which is comparable with that of pure RuO_2 shown in Fig. 5. However the trend does not continue with increase in F content and it can be seen that the current density unfortunately decreases with continued increase in F content above 10 wt% F (Fig. 7 for (Sn,Ru)O_2:F containing 15 wt% F) which potentially could arise due to the phase separation of SnO_2 from (Sn,Ru)O_2:F as observed in the XRD pattern shown in Fig. 2b. The Tafel slope of (Sn,Ru)O_2:F with 0, 5, and 10 wt% F (Table 1), calculated from the corresponding iR_Ω corrected Tafel plots, are 76, 67, 65 mV $decade^{-1}$, as shown in Fig. 8(a)–(c), respectively. This suggests that the electrochemical activity of (Sn,Ru)O_2:F increases with increase in F with the corresponding decrease in the Tafel slope for increasing F content reaching an optimal value for $(Sn_{0.8}Ru_{0.2})O_2$:10F thus exhibiting comparable electrochemical activity to that of pure RuO_2. These results therefore clearly suggest that (Sn,Ru)O_2:F containing 10 wt% F nominal composition is indeed a promising candidate as an OER anode electro-catalyst for PEM based water electrolysis. It should be noted that although the exact amount of F incorporated in the structure cannot be detected using EDAX analysis, it is nevertheless clear that with increasing amount of F there is significant increase in the electrochemical activity reaching an optimal value for the nominal composition of the oxide containing 10 wt% F.

In order to study the electrochemical stability/durability of the anode electro-catalyst (Sn,Ru)O_2:F in 1 N H_2SO_4 during OER, chronoamperometry (CA) test is conducted for 12 h at 40 °C at a constant voltage of 1.5 V, the standard accepted potential for estimating electrochemical activity. Hence this was also selected as the potential for determining the current density for assessing the degradation or loss of activity of the catalyst as a function of time in CA studies. The CA curves, obtained at a constant voltage 1.5 V, for (Sn,Ru)O_2:10 wt% F combined with that of pure RuO_2 are shown in Fig. 9. The CA curve clearly shows a decrease in current (after iR_Ω correction) with time which may be due to either dissolution of the irregular coating located at the edge of the mud cracks [15], diffusion controlled reaction or evaporation induced loss of electrolyte.

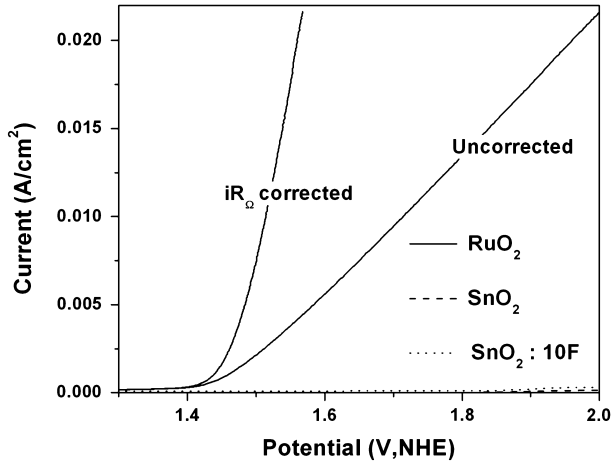

Fig. 5. The polarization curve of pure RuO_2, SnO_2 and SnO_2:10F film conducted in the presence of 1 N H_2SO_4 solution at 40 °C with a scan rate of 1 mV s^{-1} before and after iR_Ω correction.

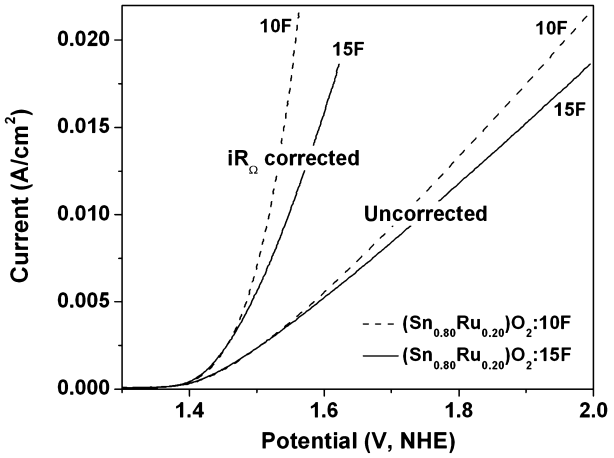

Fig. 7. The polarization curve of $(Sn_{0.8}Ru_{0.2})O_2$:15F film along with $(Sn_{0.8}Ru_{0.2})O_2$:10F conducted in the presence of 1 N H_2SO_4 solution at 40 °C with a scan rate of 1 mV s^{-1} before and after iR_Ω correction.

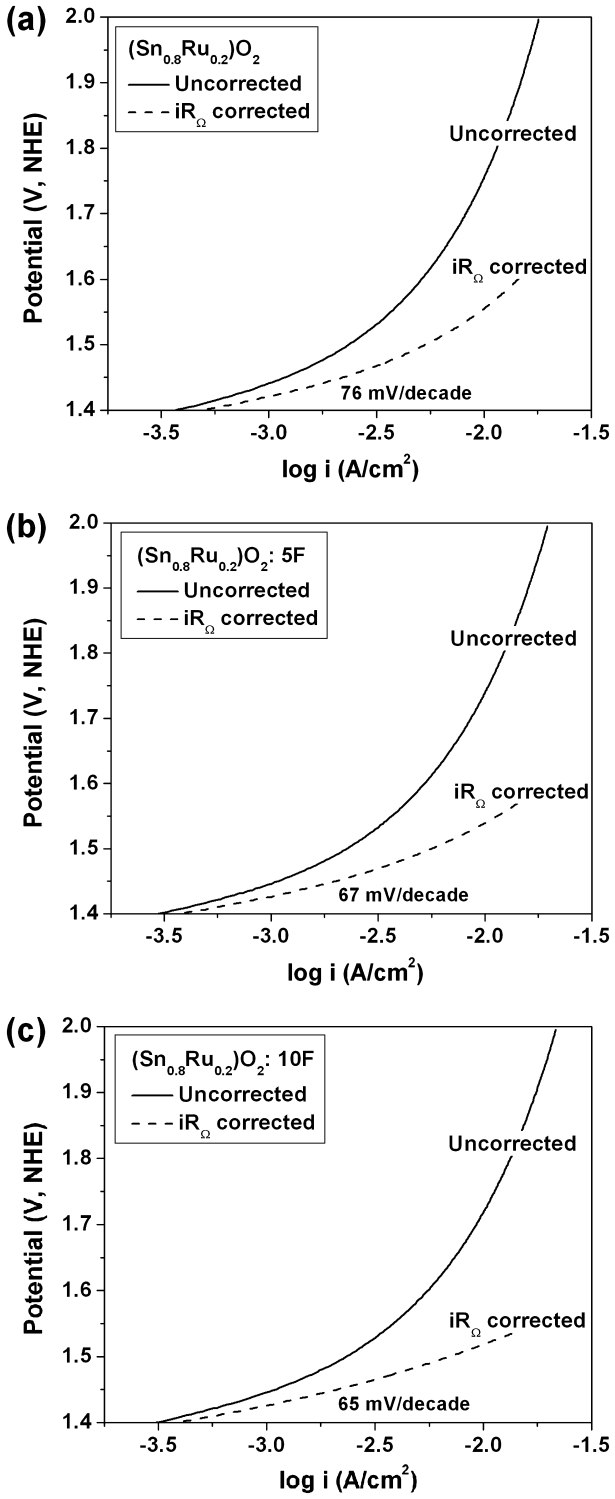

Fig. 8. The Tafel plot of (a) $(Sn_{0.8}Ru_{0.2})O_2$, (b) $(Sn_{0.8}Ru_{0.2})O_2$:5F (b) and (c) $(Sn_{0.8}Ru_{0.2})O_2$:10F, before and after iR_Ω correction, showing the Tafel slope ~76, 67 and 65 mV dec^{-1}, respectively.

A steady decrease in current has been noticed after 2 h of the initial period for both $(Sn,Ru)O_2$:10 wt% F and pure RuO_2 which suggests that $(Sn_{0.8}Ru_{0.2})O_2$:10F has similar structural stability compared to pure RuO_2. However, the ICP analysis conducted in the 1 N H_2SO_4 electrolyte solution collected after 12 h of CA measurement, shows no presence of Ru up to 10 wt% F which suggest that the steady

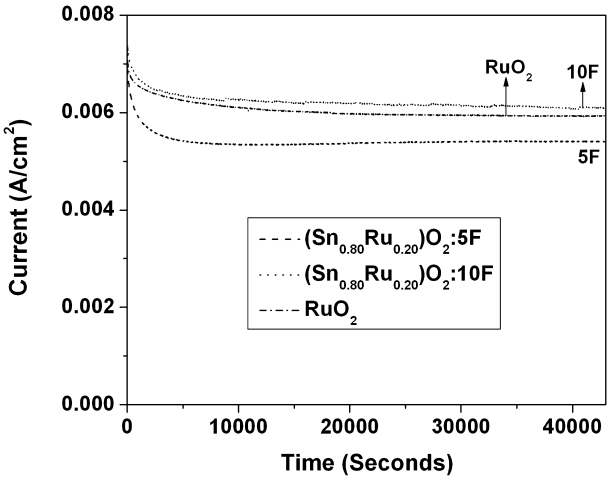

Fig. 9. The variation of current vs. time in the chronoamperometry test of pure RuO_2 and $(Sn_{0.80}Ru_{0.20})O_2$:F performed in a 1 N H_2SO_4 solution under ~1.5 V at 40 °C.

decrease in current for RuO_2 and $(Sn_{0.8}Ru_{0.2})O_2$:10F during the CA measurement (Fig. 9) may arise due to loss of fuel rather than dissolution of the Ru from the RuO_2 or $(Sn_{0.8}Ru_{0.2})O_2$:10F electro-catalyst present on the surface of the electrode. However, it has been noticed from ICP analysis that Sn is leached out in minute amounts in the solution. Solutions of $(Sn_{0.8}Ru_{0.2})O_2$:F with 0, 5 and 10 wt.% F after 12 h of CA contained 0.253 ppm, 0.227 ppm and 0.202 ppm of Sn, respectively.

Theoretical studies were also conducted to provide a fundamental understanding of this excellent electrochemical activity. We have thus explored a well known concept proposed by Nørskov et al. [50,51] that a gravity center of the d-band of the noble metal ε_d may serve as a simple descriptor for determining the catalytic activity of the surface. Such a d-band center is usually located in the vicinity of the Fermi level and an optimal position of the d-band center would provide an optimal interaction between the catalytic surface and the various species participating in the catalytic reactions predominantly occurring on the surface. Thus, an adjustment of the d-band center position with respect to the Fermi level may likely play a critical role in contributing to the design of novel highly active and electrochemically stable electro-catalysts discussed herein.

For these purposes the electronic structures of all the above mentioned Ru-based oxides have been calculated and the positions of the corresponding Ru d-band centers have been obtained as a first moment of $nd(E)$: $\varepsilon_d = \int n_d(E)E\ dE / \int n_d(E)\ dE$. Fig. 10 shows partial Ru d-band densities of states together with the corresponding centers of these zones marked with vertical arrows on the graphs. One can see that the d-band center for pure RuO_2 is located around −0.39 eV below the Fermi level. This position will be considered as a reference point for comparison of the catalytic activities of all of the other compounds experimentally explored and correspondingly simulated in this theoretical study. Gradual introduction of increased amount of Sn (up to 75 at %) to the oxide results in a hybridization between the Sn 5s, 5p and Ru 4d-states leading to a shift of the Ru d-band center up to the position at −0.22 eV below the Fermi level indicating that in general, an overall chemisorptions reaction of different species reacting at the surface becomes noticeably stronger with increase of Sn-concentration rather than for pure RuO_2 oxide.

Assuming that pure RuO_2 demonstrates an optimal catalytic activity corresponding to $\varepsilon_d = -0.39$ eV one can therefore suggest that a significant drop in the electrochemical activity observed

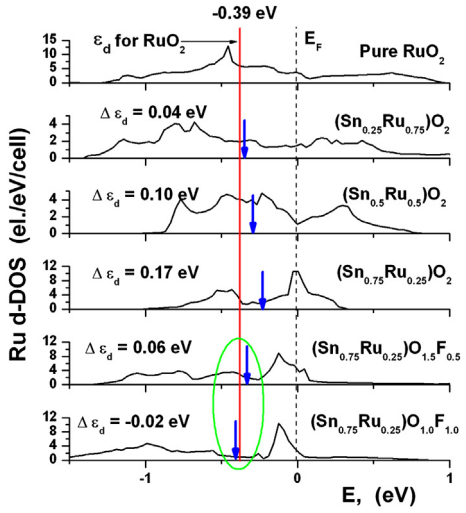

Fig. 10. Ru d-band partial DOS for the following materials: RuO_2, $(Sn,Ru)O_2$ and $(Sn,Ru)O_2$:F. Arrows denote positions of the d-band centers, ε_d.

experimentally for $(Sn_{0.8}\ Ru_{0.2})O_2$ composition (Fig. 6) could be most likely explained by a positive shift of the Ru d-band center deviating the catalytic activity from its optimal value. Such a behavior of the d-band center could be attributed to complex hybridization of the electronic Ru d-states and corresponding s and p states of Sn and O during formation of the binary oxide solid solution.

The effects of fluorine doping on the catalytic activity of the materials also can be in general considered from the electronic structure point of view and correspondingly, the d-band center shifting, in particular. Thus it can be seen from Fig. 10 that for 6.4 wt % F and 12.7 wt% F there is a gradual movement of the d-band center resulting in ε_d almost matching that of RuO_2. Fig. 11 shows the total and partial DOS for $(Sn_{0.75}Ru_{0.25})O_{1.5}F_{0.5}$ composition. Introduction of fluorine manifests in an appearance of F 2p-band mostly below −5 eV with negligible amount of other states in a whole energy region. The higher the F content, the more pronounced these 2p states are and stronger the effect of hybridization

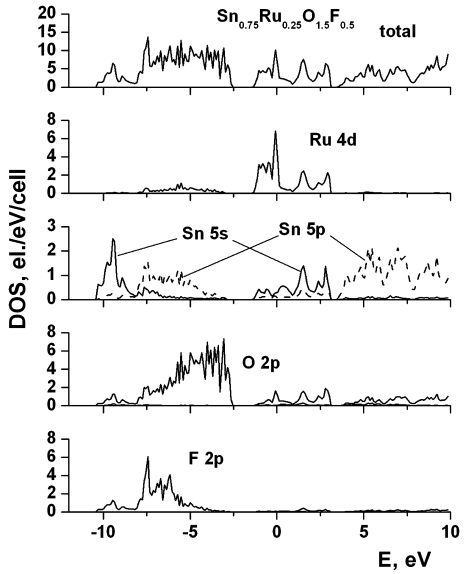

Fig. 11. Total and partial DOS for $(Sn_{0.75}Ru_{0.25})O_{1.5}F_{0.5}$.

between F 2p- and Ru 4d-states is observed. As a result, the Ru d-band center starts moving from −0.22 eV for non-fluorine composition downward toward the position corresponding to pure RuO_2 (−0.39 eV) with increase in the F content. Indeed one can therefore see that at 6.4 and 12.7 wt% of F the d-band center passes −0.33 and −0.41 eV positions, respectively, indicating an improvement in the catalytic activity with increase in the F-concentration. The optimal F-concentration at which the d-center returns back to the position corresponded to pure RuO_2 is thus expected to be around 9–10 wt% of F which is in excellent agreement with our experimental results discussed earlier in the experimental section of the manuscript.

Thus, the present theoretical study of the electronic structure peculiarities of the $(Sn,Ru)O_2$:F has demonstrated strong correlation between the d-band center position and the observed catalytic activity of the considered materials with the optimal composition corresponding to $(Sn_{0.75}Ru_{0.25})O_2$ doped with ∼10 wt% of F rendering this material to demonstrate a high catalytic activity comparable with that of pure RuO_2. This composition thus represents a substantially reduction in the noble metal content of almost 80%. Synthesis and generation of nanoparticles with similar and comparable electrochemical performance and activity would thus be the natural next step of progression and is part of the future work.

4. Conclusion

The present experimental study successfully demonstrates that F-doped $(Sn_{0.80}Ru_{0.20})O_2$ is a promising OER electro-catalyst for PEM based water electrolysis. The electrochemical performance including the current density, polarization resistance, Tafel slope and stability/durability at an optimal composition of 10 wt% F matches that of pure RuO_2. Theoretical studies comprising first-principles calculation have been performed to understand the excellent electrochemical activity of $(Sn_{0.80}Ru_{0.20})O_2$:F. The theoretical study conducted shows a positive shift of the Ru d-band center of undoped $(Sn,Ru)O_2$ with respect to pure RuO_2 thus causing deviation of the catalytic activity from its optimal value. However, incorporation of F (∼9–10 wt% F) makes the d-band center return back to the position corresponding to pure RuO_2. As a result, we conclude that $(Sn_{0.80}Ru_{0.20})O_2$:10 wt% F is potentially a preferred oxygen evolution electro-catalyst composition for water electrolysis resulting in almost ∼80% reduction in noble metal content. This system and the composition identified combined with its excellent performance can thus be considered to portend a significant reduction in the overall capital cost of PEM based water electrolyzers.

Acknowledgment

The authors gratefully acknowledge the National Science Foundation fund, Award # 0933141, the University of Pittsburgh internal funds, the Center for Complex Engineered Multi-functional Materials (CCEMM) and the Edward R. Weidlein Chair Professorship for partial financial support of this research. Finally, the authors gratefully acknowledge the support of the Pittsburgh Supercomputing Center for allocating the computational units needed to complete the theoretical component of study to support the experimental work reported in this manuscript.

References

[1] M.F. Hordeski, Hydrogen and Fuel Cells-Advances in Transportation and Power, Fairmont Press, 2009.

[2] Hydrogen Production Road Map: Technology Pathways to the Future, FreedomCAR & Fuel Partnership, Hydrogen Production Technical Team, 2009.
[3] C.J. Winter, Int. J. Hydrogen Energy 34 (2009) S1.
[4] G.W. Crabtree, M.S. Dresselhaus, M.V. Buchanan, Phys. Today 57 (2004) 39.
[5] P. Millet, N. Mbemba, S.A. Grigoriev, F.N. Fateev, A. Aukauloo, C. Etievant, Int. J. Hydrogen Energy 36 (2011) 4134.
[6] K. Zeng, D. Zhang, Prog. Energy Combust. Sci. 36 (2010) 307.
[7] F. Barbir, Solar Energy 78 (2005) 661.
[8] R.E. Clarke, S. Giddey, S.P.S. Badwal, Int. J. Hydrogen Energy 35 (2010) 928.
[9] J.I. Levene, M.K. Mann, R.M. Margolis, A. Milbrandt, Solar Energy 81 (2007) 773.
[10] A. Marshall, B. Børresen, G. Hagen, M. Tsypkin, R. Tunold, Electrochim. Acta 51 (2006) 3161.
[11] C.P. De Pauli, S. Trasatti, J. Electroanal. Chem. 396 (1995) 161.
[12] Y. Takasu, N. Yoshinaga, W. Sugimoto, Electrochem. Commun. 10 (2008) 668.
[13] S. Song, H. Zhang, X. Ma, Z. Shao, R.T. Baker, B. Yi, Int. J. Hydrogen Energy 33 (2008) 4955.
[14] X. Wu, K. Scott, Int. J. Hydrogen Energy 36 (2011) 5806.
[15] J.M. Hu, H.M. Meng, J.Q. Zhang, C.N. Cao, Corros. Sci. 44 (2002) 1655.
[16] G. Li, H. Yu, W. Song, X. Wang, Y. Li, Z. Shao, B. Li, Int. J. Hydrogen Energy 37 (2012) 16786.
[17] A.T. Marshall, S. Sunde, M. Tsypkin, R. Tunold, Int. J. Hydrogen Energy 32 (2007) 2320.
[18] J. Cheng, H. Zhang, G. Chen, Y. Zhang, Electrochim. Acta 54 (2009) 6250.
[19] V. Baglio, A. Di Blasi, T. Denaro, V. Antonucci, A.S. Aricò, R. Ornelas, F. Matteucci, G. Alonso, L. Morales, G. Orozco, L.G. Arriaga, J. New Mater. Electrochem. Syst. 11 (2008) 105.
[20] A. Marshall, B. Børresen, G. Hagen, M. Tsypkin, R. Tunold, Mater. Chem. Phys. 94 (2005) 226.
[21] G. Chen, X. Chen, P.L. Yue, J. Phys. Chem. B 106 (2002) 4364.
[22] A. Di Blasi, C. D'Urso, V. Baglio, V. Antonucci, A.S. Arico, R. Ornelas, F. Matteucci, G. Orozco, D. Beltran, Y. Meas, L.G. Arriaga, J. Appl. Electrochem. 39 (2009) 191.
[23] H. Ma, C. Liu, J. Liao, Y. Su, X. Xue, W. Xing, J. Mol. Catal. A Chem. 247 (2006) 7.
[24] J. Ailton, A.J. Terezo, J. Juan Bisquert, C. Ernesto, E.C. Pereira, G.G. Belmonte, J. Electroanal. Chem. 508 (2001) 59.
[25] X. Wu, J. Tayal, S. Basu, K. Scott, Int. J. Hydrogen Energy 36 (2011) 14796.
[26] M. Morimitsu, R. Otogawa, M. Matsunaga, Electrochim. Acta 46 (2000) 401.
[27] C.P. De Pauli, S. Trasatti, J. Electroanal. Chem. 538–539 (2002) 145.
[28] S. Ardizzone, C.L. Bianchi, G. Cappelletti, M. Ionita, A. Minguzzi, S. Rondinini, A. Vertova, Electroanal. Chem. 589 (2006) 160.
[29] E. Mayousse, F. Maillard, F. Fouda-Onana, O. Sicardy, N. Guillet, Int. J. Hydrogen Energy 36 (2011) 10474.
[30] R. Kötz, S. Stucki, Electrochim. Acta 31 (1986) 1311.
[31] C. Iwakura, K. Hirao, H. Tamura, Electrochim. Acta 22 (1977) 329.
[32] J. Ribeiro, M.S. Moats, A.R. De Andrade, J. Appl. Electrochem. 38 (2008) 767.
[33] M. Ito, Y. Murakami, H. Kaji, K. Yahikozawa, Y. Takasu, J. Electrochem. Soc. 143 (1996) 32.
[34] L.M. Da Silva, J.F.C. Boodts, L.A. De Faria, Electrochim. Acta 46 (2001) 1369.
[35] J.L. Fernandez, M.R.G. De Chialvo, A.C. Chialvo, J. Appl. Electrochem. 32 (2002) 513.
[36] M. Ito, Y. Murakami, H. Kaji, H. Ohkawauchi, K. Yahikozawa, Y. Takasu, J. Electrochem. Soc. 141 (1994) 1243.
[37] L. Nanni, S. Polizzi, A. Benedetti, A. De Battisti, J. Electrochem. Soc. 146 (1999) 220.
[38] J. Gaudet, A.C. Tavares, S. Trasatti, D. Guay, Chem. Mater. 17 (2005) 1570.
[39] L. Vazquez-Gomez, E. Horvath, J. Kristof, A. De Battisti, Thin Solid Film 515 (2006) 1819.
[40] M.K. Datta, K. Kadakia, O.I. Velikokhatnyi, P. Jampani, S.J. Chung, J.A. Poston, A. Manivannan, P.N. Kumta, J. Mater. Chem. A 1 (2013) 4026.
[41] T.H. de Keijser, J.I. Langford, E.I. Mittemeijer, A.B.P. Vogels, J. Appl. Crystallogr. 15 (1982) 308.
[42] M.K. Datta, Synthesis and Characterization of Fe–Ni–Si System Synthesized by Mechanical Alloying (Ph.D. thesis), Indian Institute of Technology, Kharagpur, India, 2002.
[43] E. Rasten, G. Hagen, R. Tunold, Electrochim. Acta 48 (2003) 3945.
[44] N. Krstajic, S. Trasatti, J. Appl. Electrochem. 28 (1998) 1291.
[45] A. Minguzzi, F.F. Fan, A. Vertova, S. Rondinini, A.J. Bard, Chem. Sci. 3 (2012) 217.
[46] G. Kresse, J. Furthmuller, Phys. Rev. B 54 (1996) 11169.
[47] G. Kresse, J. Furthmuller, Comput. Mater. Sci. 6 (1996) 15.
[48] G. Kresse, D. Joubert, Phys. Rev. B 59 (1999) 1758.
[49] J.P. Perdew, Y. Wang, Phys. Rev. B 33 (1986) 8800.
[50] B. Hammer, J.K. Nørskov, Adv. Catal. 45 (2000) 71.
[51] T. Bligaard, J.K. Nørskov, Electrochim. Acta 52 (2007) 5512.